Journal of Power Sources 264 (2014) 333–343

Contents lists available at ScienceDirect

Journal of Power Sources

journal homepage: www.elsevier.com/locate/jpowsour

Additives and salts for dye-sensitized solar cells electrolytes: what is the best choice?

Federico Bella [a,b,*], Adriano Sacco [a], Diego Pugliese [a,b], Marco Laurenti [a,b], Stefano Bianco [a]

[a] Center for Space Human Robotics @Polito, Istituto Italiano di Tecnologia, Corso Trento 21, 10129 Torino, Italy
[b] Department of Applied Science and Technology – DISAT, Politecnico di Torino, Corso Duca degli Abruzzi 24, 10129 Torino, Italy

HIGHLIGHTS

- Iodide/triiodide redox shuttle is the most studied electrolyte system for DSSCs.
- Specific salts and additives are usually introduced to improve cell efficiency.
- For the first time, chemometrics explains the real role of such components.
- Many salts and additives were investigated, maximizing cell performances.
- Efficiencies up to 10.79% were obtained by combining optimal electrolyte and blocking layer.

GRAPHICAL ABSTRACT

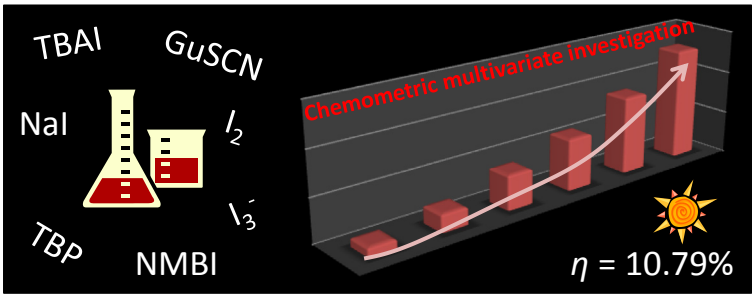

ARTICLE INFO

Article history:
Received 4 February 2014
Received in revised form
14 April 2014
Accepted 19 April 2014
Available online 30 April 2014

Keywords:
Dye-sensitized solar cell
Liquid electrolyte
Iodide
4-*tert*-Butylpyridine
Guanidinium thiocyanate
Design of experiments

ABSTRACT

A multivariate chemometric approach is proposed for the first time for performance optimization of I^-/I_3^- liquid electrolytes for dye-sensitized solar cells (DSSCs). Over the years the system composed by iodide/triiodide redox shuttle dissolved in organic solvent has been enriched with the addition of different specific cations and chemical compounds to improve the photoelectrochemical behavior of the cell. However, usually such additives act favorably with respect to some of the cell parameters and negatively to others. Moreover, the combined action of different compounds often yields contradictory results, and from the literature it is not possible to identify an optimal recipe. We report here a systematic work, based on a multivariate experimental design, to statistically and quantitatively evaluate the effect of different additives on the photovoltaic performances of the device. The effect of cation size in iodine salts, the iodine/iodide ratio in the electrolyte and the effect of type and concentration of additives are mutually evaluated by means of a Design of Experiment (DoE) approach. Through this statistical method, the optimization of the overall parameters is demonstrated with a limited number of experimental trials. A 25% improvement on the photovoltaic conversion efficiency compared with that obtained with a commercial electrolyte is demonstrated.

1. Introduction

In today's world, energy is one of the core topics: economy and political stability of nations are closely linked to the availability of fuels, and this has stimulated the international scientific

* Corresponding author. Center for Space Human Robotics @Polito, Istituto Italiano di Tecnologia, Corso Trento 21, 10129 Torino, Italy. Tel.: +39 0110903448.
E-mail address: federico.bella@polito.it (F. Bella).

http://dx.doi.org/10.1016/j.jpowsour.2014.04.088
0378-7753/

community to develop new technologies and new materials for energy production, conversion and storage [1]. As an alternative to the potential depletion of traditional fossil fuels, great attention is now devoted to the exploitation of renewable energy resources, on which man will have to rely more and more in the coming decades [2,3]. Among all, solar energy conversion is considered the most credible and viable way to face the growing energy demand, both for its high intensity (1004 W m^{-2} at ground level with the sun directly overhead) and equitable geographical distribution [4]. What is sure is that the scientific community is working hard trying to improve and optimize all of these technologies, as can be found by doing a simple search on scientific databases like Scopus: there are about 10,000 publications about "solar energy" for each of the recent years.

One of the most intriguing, exciting and promising technology developed for the sunlight conversion is the dye-sensitized solar cell (DSSC), invented by B. O'Regan and M. Grätzel 23 years ago [5,6]. Being composed merely by conductive glasses, a porous wide band gap semiconductor, a molecular dye and a redox couple dissolved in a common organic solvent, the DSSC made headlines as costing orders of magnitude less than the then-leading technology based on silicon [7]. Furthermore, the DSSCs solved a limiting problem typical of the first generation of photovoltaic devices (i.e., Si-based cells), which was the capability of operating only under perfect irradiation conditions: on the contrary, the molecular architecture of the DSSC allows the sunlight conversion even during cloudy days, thus making this technology suitable for countries with climates in which the silicon technology would never have success [8].

Right from their birth, DSSCs have been the object of many studies and, being composed of many different materials, have allowed groups with varied scientific backgrounds to engage in proposing new ingredients in order to investigate and optimize their photovoltaic performance. With this approach, great results have been achieved concerning molecular engineering of the dyes [9], incorporating novel semiconductor materials [10], the replacement of platinum with alternative cathodic materials [11], the introduction of new redox couples [12] and the flexibilization of the devices [13].

Among all the DSSC components, the electrolyte is that on which the scientific community is working hardest. Although great efforts have been focused on the introduction of quasi-solid [14] or solid [15] polymeric matrices to thwart the volatility of the organic solvents traditionally used, it must be said that the DSSCs which are entering the market are all liquid junction-based devices. For this reason, the selection of the components of the liquid electrolyte and their optimization are key factors to achieve high performance; moreover, one must be able to invest in the truly effective additives, in order to contain the cost of the final device. This justifies the large amount of work done in the field of liquid electrolytes, which has been discussed in several review articles [16–20].

A long list of additives has been proposed over the years, and it has often been observed that an additive acts favorably only on a specific photovoltaic cell parameter, but negatively on another/others. Thus, the need to adopt mixtures of two or more additives arose in order to maximize each of the cell parameters. However, as recently reported by L. Kloo, a leading expert in the field of liquid electrolytes for DSSCs, an optimum solution has not yet been identified [20]. This is due to the fact that the combination of many additives and their investigation over a wide range of concentration would require an immense amount of work, and it would also be difficult to identify quantitative relationships between different additives. In this context, our work aims to provide a valuable solution to this problem. We have conceived and implemented a multivariate experimental design able to statistically and quantitatively study the effect of different additives (each with its own experimental domain) on the cell parameters, with the goal to ascertain which additives are truly useful and which ones are irrelevant or even counterproductive. Through this chemometric approach, completely innovative in the field of liquid electrolytes for DSSCs, we were able to identify the best formulation among the many possible combinations. By joining the optimization procedure in the formulation of the electrolyte with the use of an *ad hoc* prepared blocking layer able to reduce the recombination of charges at the electrode/electrolyte interface, we demonstrated a 25% improvement on the photovoltaic performance of the device compared with the results obtained with a commercially available electrolyte.

2. Experimental

2.1. Materials

Sodium iodide (NaI), tetrabutylammonium iodide (TBAI), iodine (I_2), *N*-methylbenzimidazole (NMBI), 4-*tert*-butylpyridine (TBP), guanidinium thiocyanate (GuSCN) and acetonitrile (CH_3CN) were purchased from Sigma–Aldrich (Milan, Italy).

Conducting glass plates (FTO glass, fluorine-doped tin oxide overlayer, sheet resistance 7 Ω sq^{-1}, purchased from Solaronix, Aubonne, Switzerland) were cut into 2 × 2 cm^2 sheets and used as a substrate for the deposition of a TiO_2 porous film from a paste (DSL 18NR-AO, Dyesol Italia S.r.l., Rome, Italy) and for the fabrication of platinized counter-electrodes. Sensitizing dye *cis*-diisothiocyanato-bis(2,2′-bipyridyl-4,4′-dicarboxylato) ruthenium(II) bis(tetrabutylammonium) (N719, Ruthenizer 535 bis-TBA) was purchased from Solaronix.

2.2. Liquid electrolytes preparation

Salts and additives used for the preparation of the liquid electrolytes investigated in this work were dissolved in acetonitrile inside small glass vessels, and maintained under stirring at room temperature for 12 h. Then, the vessels were kept in the dark for one month, and no precipitation or color change was observed.

After 30 days, the measurement of the ionic conductivity and the evaluation of the photovoltaic performance in DSSC were performed. As regards the ionic conductivity, it was measured with a CyberScan PCD 650 instrument (Eutech Instruments Pte Ltd., Singapore).

The performances of the liquid electrolytes prepared were compared with those of a commercially available one: Iodolyte AN-50 (Solaronix), intended for high performance cells and widely used by the scientific community.

2.3. Preparation and characterization of TiO_2 blocking layer

Titanium dioxide (TiO_2) blocking layers were deposited by the reactive magnetron sputtering technique (Elettrorava, Turin, Italy). FTO-covered glasses were used as transparent conductive substrates, while Si wafers were used for performing cross-sectional imaging of the as-deposited materials. Before starting the deposition process, all the substrates were properly cleaned with acetone and ethanol in an ultrasonic bath and then with a Piranha solution. TiO_2 blocking layers were grown from a metallic Ti target with a target-to-substrate distance of about 8 cm, starting from a base vacuum pressure of 4 × 10^{-5} Pa. Depositions were carried out in a mixed atmosphere of Ar (95%) and O_2 (5%), at a fixed pressure value of 0.66 Pa. The RF power (13.56 MHz) was fixed to 100 V. Blocking layers were deposited for 240 min at room temperature, that is no intentional heating was provided to the substrates. To prevent any incorporation of contaminants in the films, the target was cleaned

with a 15 min sputtering process in a pure Ar atmosphere before the deposition.

The morphology and the average thickness of TiO_2 blocking layers were evaluated by means of Field Emission Scanning Electron Microscopy (FESEM), with a Carl Zeiss (Oberkochen, Germany) Double Beam Auriga instrument. The crystal structure and orientation of the blocking layers were analyzed performing X-Ray Diffraction (XRD) measurements by using a Panalytical (Almelo, The Netherlands) X'Pert MRD PRO diffractometer in parallel beam configuration. A Cu-$K\alpha$ monochromatic radiation was used as the X-ray source with $\lambda = 1.54059$ Å.

2.4. Fabrication and testing of DSSCs

As regards the preparation of photoanodes, FTO-covered glasses were rinsed with acetone and ethanol in an ultrasonic bath for 10 min. A TiO_2 paste layer with a circular shape was deposited on FTO by the doctor-blade technique and dried at 100 °C for 10 min on a hot plate. Then, a sintering process at 520 °C for 30 min allowed the formation of a mesoporous TiO_2 film with a mean thickness of 8 μm, measured by profilometry (P.10 KLA-Tencor Profiler, Milpitas, California). Finally, photoelectrodes were soaked into a 0.4 mM N719 dye solution in ethanol for 12 h at room temperature, and then rinsed in ethanol to remove the unadsorbed dye molecules.

Counter-electrode FTO glasses were cleaned with the same rinsing method described above. Two small pinholes were drilled on each FTO/glass piece through a powder blasting technique, and a 5 nm-thick Pt film was deposited onto the substrates by thermal evaporation.

DSSCs were fabricated employing a microfluidic architecture developed in our laboratory [21,22], and illustrated in Fig. 1. It consists of a polydimethylsiloxane (PDMS) thin membrane reversibly sealed between the two electrodes, with an external polymethylmethacrylate (PMMA) clamping system. The cell filling with each of the liquid electrolytes prepared in this work was performed with a syringe connected to the microfluidic housing ports and the right self-confinement of the electrolyte during the cell assembling procedure was guaranteed by the structure of the microchannels which connected the ports and the chamber. Copper foils (50 μm-thick) were used as electrical contacts with FTO.

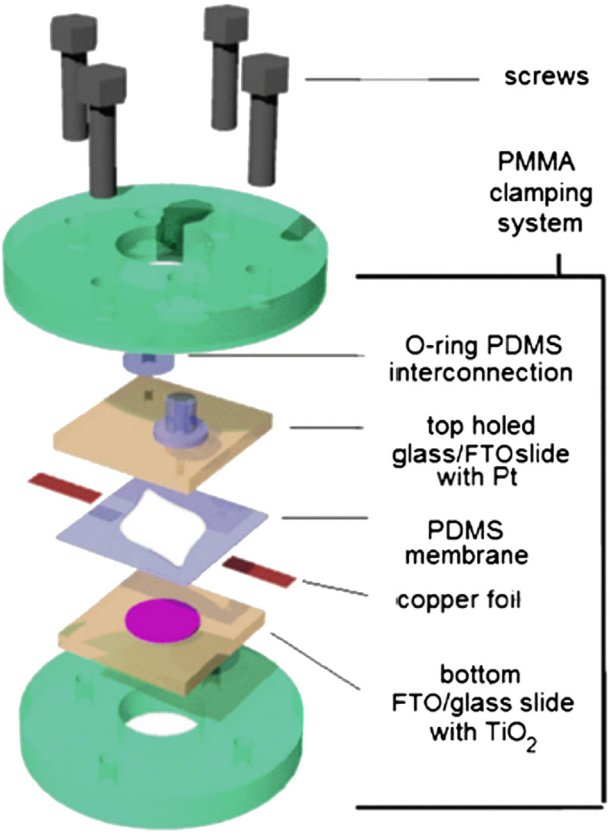

Fig. 1. Microfluidic architecture used for the assembly of DSSC. Figure reprinted from ref. 22.

The active area of the cell was 0.78 cm^2 and the photovoltaic measurements were performed with a 0.22 cm^2 rigid black mask. *I–V* electrical characterizations under AM1.5G illumination (100 mW cm^{-2}, [23,24]) were carried out using a class A solar simulator (91195A, Newport, Irvine, California) and a Keithley Instruments Inc. 2440 (Solon, Ohio) source measure unit. For the best-performing cell, *I–V* measurements were also performed at light intensities in the range of 0.2–1.0 sun, by using neutral density filters purchased from Newport. When specified, a mirror was placed under the DSSC with the aim of studying the effect of a back-scattering substrate on the photovoltaic performance.

Incident Photon-to-electron Conversion Efficiency (IPCE) measurements were performed in DC mode using a 100-W QTH lamp (Newport) as light source and a 150-mm Czerny Turner monochromator (Omni-λ 150, Lot-Oriel, Darmstadt, Germany).

The Electrochemical Impedance Spectroscopy (EIS) technique was employed to study the effect of the electrolyte additives on the charge transfer processes occurring inside the fabricated devices [25]. By employing a Metrohm Autolab BV PGSTAT128 potentiostat (Utrecht, The Netherlands) equipped with a FRA32M module, a sinusoidal signal of 10 mV with frequency variable in the range 10^{-1}–10^4 Hz was applied to the cells superimposed to a constant voltage (5 different bias voltages were tested for each devices), and the impedance was measured as a function of the frequency. The measured spectra were fitted exploiting an equivalent electrical circuit [26]. From the fitting parameters back reaction resistance (R_{br}) and chemical capacitance (C_μ), the electron lifetime (τ_n) values were calculated through the formula:

$$\tau_n = R_{br} C_\mu \quad (1)$$

2.5. Chemometric approach

As a mathematical approach to convert experimental data into useful information for decision-making in science, chemometrics is one of today's most interesting scientific disciplines [27]. Its application can be divided into two branches: the first is experiment planning to obtain the maximum information with the minimum number of trials (Design of Experiments, DoE) [28]; the second is the analysis and identification of patterns in large sets of raw experimental data to classify them (pattern recognition, PC) [29]. All this is done to counteract the strong imbalance between the technical ability to generate a large number of excellent experimental data and the human ability to properly interpret them.

As reported in Section 1, many factors combine to influence the photovoltaic performance of DSSCs assembled with different liquid electrolytes, and their combination on different levels would require thousands of experiments, as well as a highly complicated subsequent analysis. Thus, the aim of this study is to adopt a DoE approach in order to quantitatively investigate at the same time:

- the effect of the cation size in iodine salts;
- the effect of the iodide/iodine ratio;
- the effect of the concentration of V_{oc}-improver additives;
- the effect of the type of V_{oc}-improver additives;

- the effect of GuSCN, an additive on which the literature is uncertain as to its effective advantage, if any.

The multivariate DoE analysis was performed by adopting the software MODDE (version 7.0.0.1, Umetrics, Umeå, Sweden), widely used in industrial chemistry [30] and materials science [31].

3. Results and discussion

3.1. Design of experiments (DoE): matrix and measurements

The first critical step in the planning of a DoE is the definition of the variables and their experimental domain. Based on our previous experience and on the analysis of the wide literature data on liquid electrolytes for DSSCs [16–20], we selected the variables listed in Table 1.

An experimental domain as the one considered here and presented in Table 1 can be investigated by means of a fractional factorial design from the Graeco-Latin square family (FFD-GL). It is very well known that a fractional factorial design consists of a carefully chosen subset (fraction) of the experimental runs of a full factorial design, which is a typically used DoE [32]. As regards the Graeco-Latin square (of order n over two sets S and T, each consisting of n symbols), it is an $n \times n$ arrangement of cells, each cell containing an ordered pair (s,t), where s is in S and t is in T, such that every row and every column contains each element of S and each element of T exactly once, and that no two cells contain the same ordered pair [33]. FFD-GL is a three levels fractional factorial design useful to investigate a system with up to 13 variables: for this reason, it has been chosen for this work, and each of the variables listed in Table 1 has been investigated at 3 levels (−1, 0, +1), with a total of 30 experiments, as reported in Table 2. The detailed statistical bases of the selected DoE can be found in ordinary books of applied statistics [34].

The proper selection of the components of liquid electrolytes for DSSCs and the resulting performances on lab-scale devices were investigated by means of an FFD-GL DoE, a multivariate analysis method which permits the optimization of the investigated system, simultaneously determining variables as others are modified. With this mathematical technique, the six operational variables reported in Table 1 were simultaneously considered in order to identify the weight of each one and the relationship between them, indicating synergies and antagonisms.

As reported in Table 2, 30 experiments were carried out, and the following parameters (experimental responses) were measured: sunlight conversion efficiency (η, %), short-circuit current density (J_{sc}, mA cm^{-2}), open-circuit voltage (V_{oc}, mV), fill factor (FF), chemical capacitance (C_{μ}, F cm^{-2}), effective electron lifetime (τ_n, s) and ionic conductivity of the liquid electrolyte (σ, mS cm^{-1}). The values of these experimental responses for the 30 DSSCs are reported in Table 3 (J_{sc}, V_{oc}, FF, η, σ) and Table S1 (C_{μ}, τ_n). As a comparison, a cell was assembled with one of the most well-known commercial liquid electrolytes (Iodolyte AN-50, Solaronix); its performance is included in the last row of Table 3.

After carrying out the experimental runs, the chemometric approach plans to perform the fit of the model. In the present system, several responses were measured, as detailed above. In this case, it is useful to fit the model simultaneously representing the variation of all the responses to the variation of the factors of Table 1: we selected the Partial Least Squares (PLS) method, which deals with many responses simultaneously, taking their covariances into account. PLS method has been extensively described in the literature, and a simple tutorial can be found elsewhere [35]. Calculated interpolation parameters for our model were $R^2 = 0.95$ and $Q^2 = 0.92$. As is well known, R^2 represents the fraction of the response variation explained by the model and Q^2 is the fraction of the response variation that can be predicted by the model. More generally, R^2 and Q^2 provide the summary of the fit of the model: R^2 is an overestimated measure and Q^2 an underestimated value of the exactness of the fit of the model. Both of these values are very close to 1, meaning that the regression model provides an excellent description of the relationship between the independent variables and the responses, and therefore an optimal analysis of the investigated system. A further plot useful for evaluating the exactness of the chemometric model is shown in Fig. S1, where the absence of outliers is shown in a normal probability plot of residuals.

As regards the experimental reproducibility, it was evaluated by two different approaches. The experiment with all the variables at their intermediate level has been reproduced three times, as can be seen in runs N28–N30 (Table 2). If we focus on the most important response (η), it can be easily calculated from Table 3 that the average value of sunlight conversion efficiency for the three replicated cells is 5.51 (±0.15)%: this value is not only an excellent index of reproducibility if compared to the repeatability typically observed in the literature for DSSCs [36], but it also perfectly corresponds to the theoretical value predicted by the chemometric

Table 1
Variables and relative experimental domains selected for projecting the DoE.

Variable	Symbol	Experimental domain	Description
x_1	[I$^-$]	0.30–0.60 M	Iodide concentration
x_2	x_{NaI}	0–1	Molar fraction of NaI (the rest is TBAI)
x_3	I$^-$/I$_2$	8–12	Iodide/Iodine molar ratio
x_4	[V_{oc}-imp]	0.40–0.70 M	Concentration of V_{oc}-improver additives
x_5	x_{TBP}	0–1	Molar fraction of TBP (the rest is NMBI)
x_6	[GuSCN]	0–0.40 M	Concentration of GuSCN

Table 2
FFD-GL model matrix composed of 30 experiments useful to investigate the 6 variables of Table 1. Coded values for each variable are reported in brackets.

Exp. Name	x_1 (M)	x_2	x_3	x_4 (M)	x_5	x_6 (M)
N1	0.30 (−1)	0 (−1)	8 (−1)	0.40 (−1)	0 (−1)	0 (−1)
N2	0.30 (−1)	0 (−1)	8 (−1)	0.40 (−1)	0.5 (0)	0.2 (0)
N3	0.30 (−1)	0 (−1)	8 (−1)	0.40 (−1)	1 (+1)	0.4 (+1)
N4	0.30 (−1)	0.5 (0)	10 (0)	0.55 (0)	0 (−1)	0 (−1)
N5	0.30 (−1)	0.5 (0)	10 (0)	0.55 (0)	0.5 (0)	0.2 (0)
N6	0.30 (−1)	0.5 (0)	10 (0)	0.55 (0)	1 (+1)	0.4 (+1)
N7	0.30 (−1)	1 (+1)	12 (+1)	0.70 (+1)	0 (−1)	0 (−1)
N8	0.30 (−1)	1 (+1)	12 (+1)	0.70 (+1)	0.5 (0)	0.2 (0)
N9	0.30 (−1)	1 (+1)	12 (+1)	0.70 (+1)	1 (+1)	0.4 (+1)
N10	0.45 (0)	0 (−1)	10 (0)	0.70 (+1)	0 (−1)	0.2 (0)
N11	0.45 (0)	0 (−1)	10 (0)	0.70 (+1)	0.5 (0)	0.4 (+1)
N12	0.45 (0)	0 (−1)	10 (0)	0.70 (+1)	1 (+1)	0 (−1)
N13	0.45 (0)	0.5 (0)	12 (+1)	0.40 (−1)	0 (−1)	0.2 (0)
N14	0.45 (0)	0.5 (0)	12 (+1)	0.40 (−1)	0.5 (0)	0.4 (+1)
N15	0.45 (0)	0.5 (0)	12 (+1)	0.40 (−1)	1 (+1)	0 (−1)
N16	0.45 (0)	1 (+1)	8 (−1)	0.55 (0)	0 (−1)	0.2 (0)
N17	0.45 (0)	1 (+1)	8 (−1)	0.55 (0)	0.5 (0)	0.4 (+1)
N18	0.45 (0)	1 (+1)	8 (−1)	0.55 (0)	1 (+1)	0 (−1)
N19	0.60 (+1)	0 (−1)	12 (+1)	0.55 (0)	0 (−1)	0.4 (+1)
N20	0.60 (+1)	0 (−1)	12 (+1)	0.55 (0)	0.5 (0)	0 (−1)
N21	0.60 (+1)	0 (−1)	12 (+1)	0.55 (0)	1 (+1)	0.2 (0)
N22	0.60 (+1)	0.5 (0)	8 (−1)	0.70 (+1)	0 (−1)	0.4 (+1)
N23	0.60 (+1)	0.5 (0)	8 (−1)	0.70 (+1)	0.5 (0)	0 (−1)
N24	0.60 (+1)	0.5 (0)	8 (−1)	0.70 (+1)	1 (+1)	0.2 (0)
N25	0.60 (+1)	1 (+1)	10 (0)	0.40 (−1)	0 (−1)	0.4 (+1)
N26	0.60 (+1)	1 (+1)	10 (0)	0.40 (−1)	0.5 (0)	0 (−1)
N27	0.60 (+1)	1 (+1)	10 (0)	0.40 (−1)	1 (+1)	0.2 (0)
N28	0.45 (0)	0.5 (0)	10 (0)	0.55 (0)	0.5 (0)	0.2 (0)
N29	0.45 (0)	0.5 (0)	10 (0)	0.55 (0)	0.5 (0)	0.2 (0)
N30	0.45 (0)	0.5 (0)	10 (0)	0.55 (0)	0.5 (0)	0.2 (0)

Table 3
Photovoltaic parameters of DSSCs assembled with the 30 liquid electrolytes proposed in Table 2, accordingly to the FFD-GL DoE. The ionic conductivity values of the liquid electrolytes are also reported (in the last column). Data of a commercial liquid electrolyte (Iodolyte AN-50) are listed in the last row.

Exp. Name	J_{sc} (mA cm^{-2})	V_{oc} (mV)	*FF*	η (%)	σ (mS cm^{-1})
N1	12.3	718	0.56	4.94	15.98
N2	12.3	672	0.58	4.83	15.51
N3	10.6	669	0.55	3.86	16.96
N4	9.78	615	0.59	3.56	16.52
N5	11.0	681	0.57	4.29	15.24
N6	10.5	669	0.49	3.45	17.44
N7	15.1	702	0.55	5.87	17.45
N8	10.4	682	0.61	4.29	16.14
N9	11.2	675	0.54	4.13	17.19
N10	13.9	723	0.57	5.75	18.02
N11	11.9	685	0.54	4.39	17.18
N12	14.5	722	0.61	6.38	18.32
N13	13.3	666	0.56	4.99	19.25
N14	12.0	667	0.60	4.85	18.95
N15	15.0	669	0.62	6.20	22.03
N16	10.5	656	0.63	4.36	21.14
N17	11.6	683	0.61	4.84	21.44
N18	16.6	668	0.62	6.90	25.31
N19	14.6	705	0.55	5.72	19.37
N20	13.9	702	0.62	6.06	20.09
N21	15.1	682	0.60	6.14	18.90
N22	11.1	685	0.62	4.69	19.31
N23	13.6	667	0.67	6.03	21.48
N24	15.1	662	0.66	6.57	22.73
N25	12.0	651	0.61	4.81	25.09
N26	13.6	650	0.63	5.57	29.41
N27	14.2	682	0.65	6.29	26.50
N28	14.4	704	0.54	5.52	18.53
N29	13.8	698	0.59	5.65	18.59
N30	14.7	709	0.51	5.35	18.54
AN-50	12.9	625	0.62	5.03	24.60

model (5.48%). As a second approach, in order to further support the statistical model, a cross-validation process was carried out: it is a model validation technique for assessing how the fitted results of a chemometric model will generalize to an independent data set. Basically, the software proposes a few new experiments to be performed, and also predicts the results to be obtained in laboratory. The validation of the chemometric model is achieved if the experimental results obtained correspond to the predicted ones within 95% confidence. This was actually the case, meaning that the chemometric model presented here is robust and valid.

The set of experiments carried out allowed us to achieve a maximum light-to-electricity conversion efficiency of 6.90% (J_{sc} = 16.6 mA cm^{-2}, V_{oc} = 668 mV, *FF* = 0.62) for the DSSC assembled with the liquid electrolyte in which: $x_1 = [I^-] = 0.45$ M, $x_2 = x_{NaI} = 1$, $x_3 = I^-/I_2 = 8$, $x_4 = [V_{oc}\text{-imp}] = 0.55$ M, $x_5 = x_{TBP} = 1$, $x_6 = [GuSCN] = 0$ M.

Fig. 2 shows the influence (with 95% confidence) of each variable on the investigated experimental responses. The coefficients have been normalized in order to allow the study of the effect of each variable on different responses; in this way, the real effect that each variable has on the photovoltaic performance of the device is shown. A detailed investigation of these effects and their interpretation will be given in the next sections.

3.1.1. Effect of iodide concentration (x_1)

Since the earliest studies [5], the iodide/triiodide couple has been the most commonly used redox mediator, due to its favorable kinetic properties. In particular, Grätzel has recently highlighted the "asymmetric behavior" of this redox mechanism, since the forward electron donation by I^- is sufficiently fast to ensure an efficient sensitizer regeneration, while the reduction of I_3^- at the photoanode is slow enough to allow for high carrier collection efficiencies [16].

The iodide concentration is a variable not easily treated, as it affects in the opposite direction the values of photocurrent and photovoltage of the resulting DSSC. As can be noted in Fig. 2B and E, the effect of increasing the iodide concentration is positive on both the J_{sc} and σ values. It is well known that the regeneration of the dye cations needs I^-, thus the increase in the cell performance while increasing the iodide concentration can be assigned to the availability of more iodide ions. In this work, we decided not to adopt iodide concentrations greater than 0.60 M because, above this value, the trends of J_{sc} and σ are reversed: this is due to the formation of ion pairs, whose mobility is severely limited and, therefore, the regeneration of the oxidized dye is inhibited [37].

On the other hand, the coefficient plot in Fig. 2C shows that the increase of the iodide concentration worsens the V_{oc}, namely the difference between the Fermi level of TiO_2 (E_F) and the redox potential of electrolyte (E), which can be expressed by the Nernst equation:

$$E = E^{\circ} - \frac{RT}{NF} ln \frac{a_R}{a_O} \quad (2)$$

where E° is the standard electrode potential, R the gas constant, T the absolute temperature, N the electron number per one reaction species, F the Faraday constant, a_R and a_O the activities of reduction and oxidation species, respectively [38]. From Eq. (2), it is easy to notice that the increase of concentration of reducing species (iodide) causes a shift of the redox potential to more negative values. As a consequence, V_{oc} decreases because the energy gap between E_F and E becomes smaller.

In summary, it is necessary to find a compromise to obtain the highest possible J_{sc} value without significantly lowering the V_{oc}. The chemometric model suggests that an optimal concentration of iodide would be 0.45 M, which is in fact the value employed for the most efficient cell (N18 in Tables 2 and 3). As a comparison, the commercial Iodolyte AN-50 liquid electrolyte (whose iodide concentration is unknown) presents a J_{sc} value (12.9 mA cm^{-2}) much lower than that of N18 cell (16.6 mA cm^{-2}), even if the ionic conductivities are almost the same (24.60 mS cm^{-1} and 25.31 mS cm^{-1}, respectively): this could mean that the commercial product also contains salts different from iodides, probably introduced as supporting electrolytes or stabilizers for particular additives.

3.1.2. Effect of iodide counterion (x_2)

The photovoltaic performance of a DSSC depends not only on the concentration of the iodide salt, but also the selected iodide counterion is relevant from a photoelectrochemical point of view. Counterions differ from each other by size and charge density: it has been reported that the photocurrent decreases and the photovoltage raises while increasing the cations radius, due to the variation of the TiO_2 conduction band energy (E_c) and the associated influence on the electron injection efficiency [39]. Moreover, it has been reported that the dye regeneration process can be accelerated by small cations (Mg^{2+}, Li^+, Na^+) [40,41].

An exhaustive study of the influence of counterions has recently been performed by Wang et al., who explored the effect of small and large ions on the photovoltaic performance of DSSCs [42]. However, a study of the effect of mixtures of salts with different counterions has never been carried out, nor the presence of other additives in the electrolyte solution containing different salts has been investigated. In the FFD-GL DoE, we considered the most used salt (NaI) and the iodide salt which usually leads to the highest V_{oc} values (TBAI), by tuning the NaI/TBAI ratio. We decided to exclude LiI from the investigation, although it is widely used by DSSC

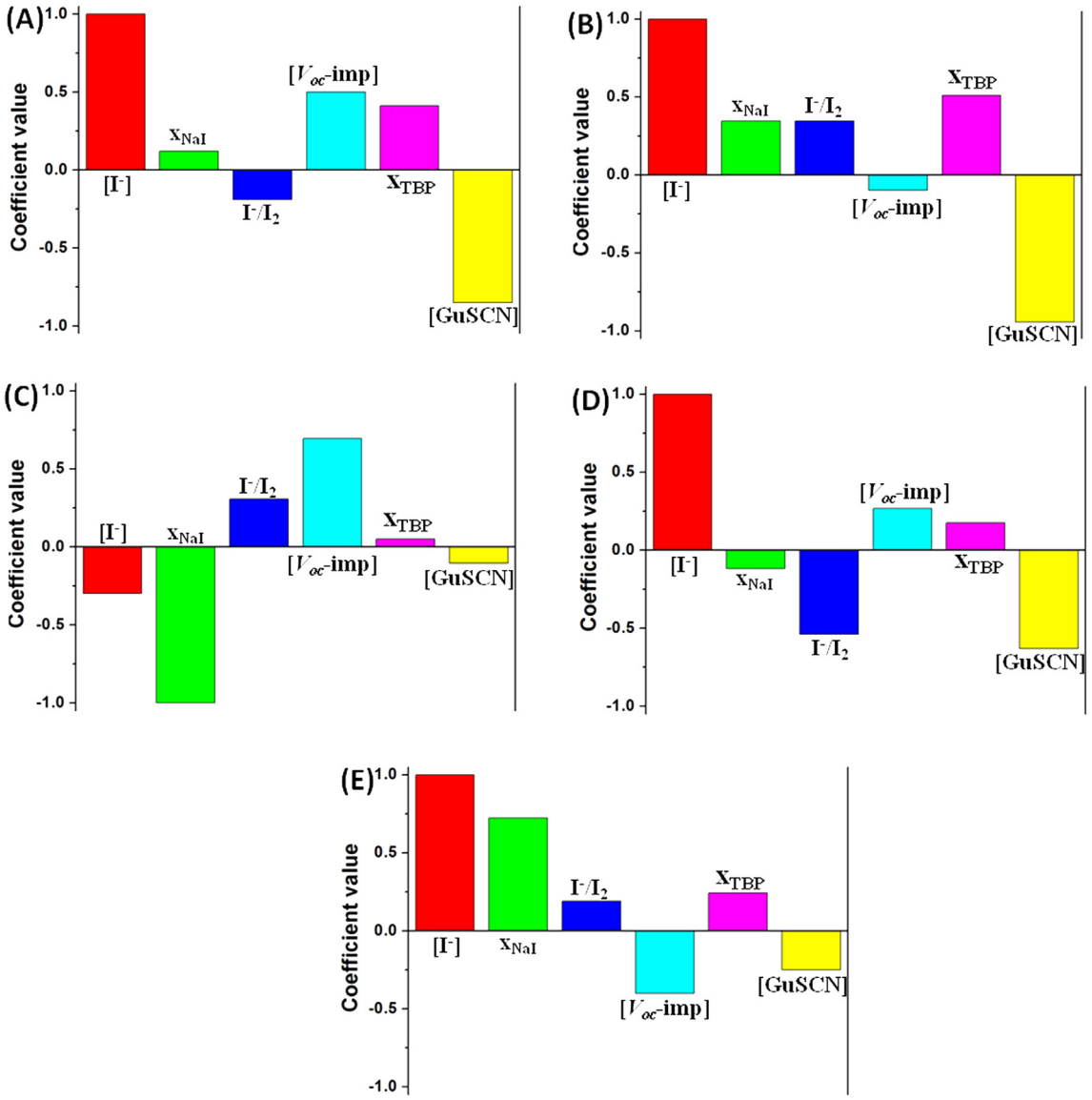

Fig. 2. Coefficient plots for the FFD-GL DoE, resulting from the fitting of the experiments reported in Table 3. Each bar indicates if the corresponding variable is acting in favor (positive value) or against (negative value) the measured experimental response. A: η; B: J_{sc}; C: V_{oc}; D: *FF*; E: σ.

community, because from our preliminary studies (consistent with others recently published, [43]) we found a huge decrease in photovoltaic performance upon intercalation of Li^+ ions into a TiO_2 nanostructured photoelectrode, causing the formation of Ti^{3+} species which trap electrons in localized states [44].

As can be noted in Fig. 2C, high values of x_{NaI} lead to lower V_{oc} values: in fact, the cells with the highest V_{oc} values (N1, N10 and N12 in Table 3) are those containing a liquid electrolyte composed almost exclusively of TBAI. This means that different cations affect the interfacial energies of dye-sensitized TiO_2 electrodes. In particular, when electrons accumulate in the TiO_2 conduction band, cations adsorb onto its surface or intercalate into its lattice for charge compensation. Therefore, a cation size-dependent drop in the Helmholtz layer occurs, which results in a negative shift of E_c values while increasing cation radius, leading to higher photovoltages. This fact is successfully confirmed by the comparison of the chemical capacitance (see Table S1) upon Na^+ adsorption (cell N26, $C_\mu = 0.11$ mF cm^{-2}) with respect to the higher value when only TBAI is used (cell N12, $C_\mu = 1.53$ mF cm^{-2}). In this last case, in fact, the larger ionic radius is responsible for the enhancement of the capacitance.

On the other hand, from Fig. 2B it can be noted that increasing the amount of NaI (with respect to TBAI) leads to better J_{sc} values. This is a direct consequence of the size of the two investigated cations. In fact, the shift of E_c produced by TBAI is more negative than that of NaI, and this causes a more pronounced decrease of the driving force necessary for the injection of electrons from the excited dye to the semiconductor. Furthermore, another factor must be considered to explain the increase of J_{sc} in the presence of NaI: the photocurrent also depends on the diffusion of the redox species, and it is well known that the mobility of little cations (Na^+) is higher than that of larger ones (TBA^+). This is due also to the fact that the larger the ion, the less it is solvated: less solvated cations can form Bjerrum-Fuoss ion pairs with I^- or I_3^- [45], resulting in reduced ion mobility and activity. This behavior is reflected in Fig. 2E, where it is evident that the ionic conductivity is higher in the presence of NaI compared to TBAI: by way of example, note that the highest conductivity obtained in the presence of NaI is

29.41 mS cm^{-1} (cell N26 in Table 3), while in the presence of TBAI it is at most 20.09 mS cm^{-1} (cell N20).

Electrolytes containing both NaI and TBAI provided good photovoltaic performance (see cells N23 and N24 in Tables 2 and 3), but a synergistic effect between the two salts was not obtained. From a quantitative point of view, Fig. 2A shows that NaI is the best salt for high-performing DSSC devices. As a comparison, from Table 3 it can be noted that the commercial Iodolyte AN-50 liquid electrolyte presents a J_{sc} value (12.9 mA cm^{-2}) much lower than that of the NaI-based N18 cell (16.6 mA cm^{-2}); furthermore, also its V_{oc} value is lower (628 mV versus 668 mV). The lower photovoltage can be explained considering that Iodolyte AN-50 contains a lithium salt: Li^+ is smaller than Na^+, and produces a less negative shift of TiO_2 E_c. As regards the lower J_{sc}, this is justified by the fact that Iodolyte AN-50 also contains ionic liquids as an iodide source: although this is favorable because of the lower toxicity and better thermal stability of ionic liquids, it is necessary to say that their mobility is lower than that of NaI and their cost is very high (12.5 € g^{-1} for 1-methyl-3-propylimidazolium iodide versus 0.55 € g^{-1} for NaI).

3.1.3. Effect of iodide/iodine ratio (x_3)

Liquid electrolytes for DSSCs usually contain a source of iodide (NaI, TBAI, ionic liquids) and iodine. The latter binds iodide to form triiodide, by means of the chemical reaction

$$I_2 + I^- \rightleftarrows I_3^- \tag{3}$$

Its equilibrium constant is very high, so that the concentration of free I_2 is very low ($\sim 10^{-8}$ M when 0.5 M I^- and 0.05 M I_2 are mixed) [18].

The amount of triiodide (or, indirectly, iodine) is very influential on the cell performance. It modifies not only the redox potential of electrolyte (E, as described by Eq. (2)), but directly affects the V_{oc} accordingly to the equation

$$V_{OC} = \frac{k_B T}{e} \ln\left(\frac{J_{\text{inj}}}{k_{rec} n_{c,0} \left[I_3^-\right]}\right), \tag{4}$$

where k_B is the Boltzmann constant, e the elementary charge, J_{inj} the flux of injected electrons, k_{rec} the rate constant for I_3^- reduction and $n_{c,0}$ the conduction band electron density in the dark. In summary, the higher the I_3^- concentration (thus, the lower the I^-/I_2 molar ratio), the lower the V_{oc}. On the other hand, it is not possible to adopt very low [I_3^-] values, since the transport of triiodide to the counter-electrode has been recognized as a rate-limiting step in DSSCs if its concentration is low (or if the solvent is viscous) [46].

On the basis of these considerations, the scientific community usually fixes a I^-/I_2 molar ratio equal to 10:1 [47]. Due to the versatility of the implemented FFD-GL DoE, we tuned the iodide/iodine ratio between 8 and 12. As can be seen from the fitted coefficient in Fig. 2A, the increase of the I^-/I_2 molar ratio negatively affected the sunlight conversion efficiency of the devices, due to a reduction in *FF* values, even if J_{sc} and V_{oc} slightly increased.

The slight decrease of V_{oc} at low I^-/I_2 molar ratios was expected according to Eq. (4), and it can be explained through an increased recombination between electrons in the conduction band of TiO_2 and triiodide ions. This hypothesis can be confirmed by looking at the electron lifetime values reported in Table S1, which are related to the charge recombination. As an example, cell N16, whose I^-/I_2 molar ratio is equal to 8, presents an open circuit voltage equal to 656 mV and a τ_n value of 8 ms. On the contrary, a cell fabricated with a higher iodide/iodine ratio (N19 in Table 2), characterized by a larger V_{oc}, exhibits a higher lifetime, equal to 120 ms, meaning a reduction of the back electron recombination.

As regards the increase of J_{sc} in the presence of high I^-/I_2 molar ratio values, it can be explained through the photophysical and photochemical behavior of triiodide. In fact, I_3^- ions strongly absorb light in the visible range, thus interfering with the light harvesting of the dye molecules [48]. This effect is much more pronounced when the I^-/I_2 ratio is low, thus justifying the observed trend. On the other hand, a low amount of I_3^- could be problematic during cell ageing: in fact, it is well known that the triiodide – under irradiation – homolytically dissociates according to the following reaction [49]:

$$I_3^- + h\nu \rightarrow I_2^{\bullet -} + I^{\bullet} \tag{5}$$

As a consequence of Eq. (5), the electrolytes with small amounts of I_3^- (i.e., those with high I^-/I_2 molar ratio) will be subjected to a further depletion of this fundamental ion; moreover, the $I_2^{\bullet -}$ ion is expected to accept electrons from the semiconductor conduction band, thus giving additional recombination.

An interesting effect of the lowering of I^-/I_2 molar ratio is the increase of *FF* values. This fact has already been studied in literature [50,51] and attributed to a decrease of the total series resistance of the DSSCs, which is responsible for an enhancement of the *FF*. In particular, the electrolyte diffusion resistance value is reduced upon increasing iodine concentrations [51], and this in turn affects the total series resistance of the cell [12].

In summary, the combined effect of I^-/I_2 molar ratio on J_{sc}, V_{oc} and *FF* was weighed in quantitative terms by the FFD-GL DoE multivariate approach, and it was deduced that a ratio equal to 8 is the best choice. This was further experimentally confirmed by comparing our best electrolyte (N18, I^-/I_2 molar ratio equal to 8, thus [I_3^-] = 56 mM) with the Iodolyte AN-50 commercial product, which contains a lower triiodide amount (50 mM).

3.1.4. Effect of V_{oc}-improver additives concentration (x_4)

From the previous sections, it has already emerged that the V_{oc} is a very important parameter in determining the overall photovoltaic performance of a DSSC. Therefore, a large amount of scientific research has been done in recent years to synthesize specific additives for the liquid electrolyte to maximize this cell parameter [20]. The most frequently used additives are nitrogen-containing heterocyclic compounds, such as pyridines, aminotriazole, pyrimidine, aminothiazole, pyrzaole and quinoline. Above all, 4-*tert*-butylpyridine, developed by Grätzel's group [52], is the most used additive. Another category of organic compounds is that of *N*-alkylbenzimidazole derivatives: they were found to behave in a similar way to TBP, so that *N*-methylbenzimidazole is also often added in liquid electrolytes both for TiO_2- [53] and ZnO-sensitized DSSCs [10].

We focused our attention on the two most widely used V_{oc}-improver additives: TBP and NMBI. By means of the chemometric approach, we decided to investigate the effect of both the concentration of V_{oc}-improver additives (in this section), and of their composition (only TBP, only NMBI, mixtures TBP-NMBI; see Section 3.1.5).

From the coefficient plot shown in Fig. 2A, a valuable increase of the sunlight conversion efficiency values in the presence of V_{oc}-improver additives is evident. The increase in V_{oc} (Fig. 2C) was expected, and it was also accompanied by a slight increase in *FF* (Fig. 2D). In fact, as well known, one of the main effects of the V_{oc}-improver additives is the enhancement of the lifetime values [10], as witnessed by the cells N12 (highest additive concentration, see Table 2) and N26 (lowest concentration). In the first case the lifetime is 144 ms, while the value is as low as 5 ms for the other cell.

While the effects of these additives on V_{oc} values are well known and several action mechanisms have been proposed (see Section

3.1.5), nothing has been said about the effect that high concentrations of these compounds would cause. In particular, it is worth noting that these additives lead to lower J_{sc} values (Fig. 2B) if present in large amounts. For example, let us consider cell N18 in Table 3, containing 0.55 M of V_{oc}-improver additives: when their concentration was increased up to 0.70 M (cell N10), the V_{oc} value was increased from 668 mV to 723 mV, while J_{sc} decreased from 16.6 mA cm^{-2} to 13.9 mA cm^{-2}. More detailed investigation showed that the addition of a large quantity of V_{oc}-improver additives to the electrolyte led to a significant decrease in the IPCE, as can be seen in Fig. 3. In particular, we observed that the IPCE did not decrease proportionally over the whole spectral range, but the difference between the two cells was stronger on the red end of the spectrum. A possible reason for this phenomenon is that the two additives (TBP and NMBI), which are basic organic compounds, led to a partial deprotonation of the N719 dye, thus resulting in a well-known blue-shifted absorption spectrum [54]. Another explanation was proposed by Boschloo et al., who supposed that the blue-shift was due to a negative shift in the conduction band edge energy of TiO_2, caused by the adsorption of TBP on the photoanode surface [55].

Such observations lead to the conclusion that it will be difficult to significantly increase the voltage output of DSSCs without sacrificing the photocurrent, but it is necessary to select an adequate value of V_{oc}-improver additives concentration, which is (from the chemometrics) 0.55 M. This concentration value allows optimizing both J_{sc} and V_{oc}, as it is evident from the data of cell N18 in Table 3, especially if compared with the values obtained for a DSSC assembled with the Iodolyte AN-50 commercial electrolyte, whose V_{oc} was 43 mV lower than that of the cell N18.

3.1.5. *Effect of V_{oc}-improver additive type (x_5)*

If in the previous section we focused on the concentration of V_{oc}-improver additives, now we consider their chemical nature. In particular, by means of the FFD-GL DoE we decided to investigate if it is better to use TBP, NMBI or a mixture thereof (x_{TBP} from 0 to 1).

The action mechanism of these nitrogen-based organic compounds has been extensively investigated in the literature. Both TBP and NMBI adsorb on the photoanode surface, shifting its band edge and acting as a barrier to the recombination at the semiconductor/electrolyte interface [56]. Some groups tried to quantify these two effects, concluding that the band edge shift of TiO_2 is responsible for 60% of the voltage increase, while the increase of the electron lifetime contributes for the 40% [57]. Furthermore, it was also demonstrated that the addition of TBP or NMBI to the electrolyte enhanced the dye lifetime at elevated temperatures and – by steric hindrance – protected it from nucleophilic attack by acetonitrile or methoxypropionitrile [58].

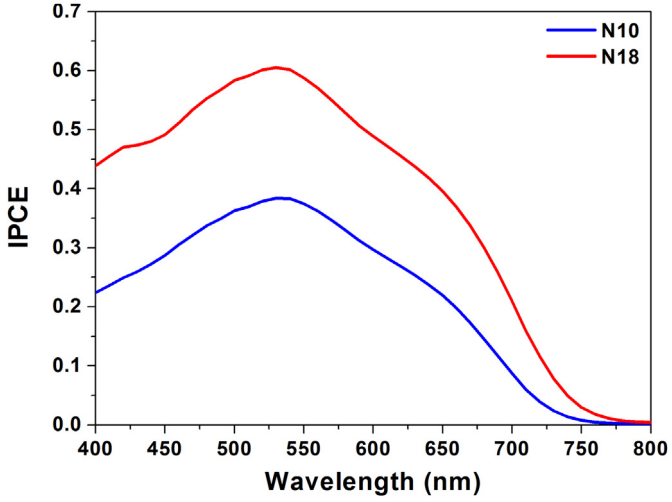

Fig. 3. IPCE curves for DSSCs assembled with liquid electrolytes containing different amounts of V_{oc}-improver additive: 0.55 M (cell N18) and 0.70 M (cell N10). IPCE values are reported in 0–1 scale.

Although the two additives have a similar action mechanism, by the experiments reported in Table 3 it is clear that TBP and NMBI led to rather different photovoltaic performance. In particular, the coefficient plots in Fig. 2 show that, despite the effect of the two additives on the V_{oc} is the same (the bar of x_{TBP} in Fig. 2C is almost nil), the NMBI led to lower efficiencies (Fig. 2A) due to a sharp decrease of J_{sc} values (the bar of x_{TBP} is very positive in Fig. 2B, meaning that NMBI acted against J_{sc}). For example, cells N16 and N18, which contain the same amount of NMBI and TBP, respectively, can be considered: the values of V_{oc} are similar (656 and 668 mV, respectively), while the J_{sc} of N16 (10.5 mA cm^{-2}) is well below than that of N18 (16.6 mA cm^{-2}). It is also interesting to note that there is a synergistic effect between TBP and NMBI on V_{oc}: cell N17 contains a 1:1 TBP:NMBI molar ratio ($x_{TBP} = 0.5$) and its V_{oc} is 683 mV, higher than those of the cells containing the two additives separately (668 and 656 mV, respectively); however, J_{sc} is quite low (11.6 mA cm^{-2}), and the resulting efficiency is lower than that of cell N18.

From these experiments, it seems that the best option is to employ only TBP as V_{oc}-improver additive, since, compared to NMBI, it leads to a minor decrease in photocurrent. This drawback of NMBI was also reported by other groups [38], but never justified. A possible explanation may be found in a recently reported periodic density functional theory study, which indicates that the increment of Fermi energy for NMBI adsorbed on the TiO_2 (101) surface is much larger than that of TBP [59]. As a consequence, NMBI could be more advantageous to heighten the open circuit photovoltage, but this also leads to lower electron injection efficiency, resulting in smaller J_{sc} values.

As regards the Iodolyte AN-50 commercial electrolyte, its composition in terms of V_{oc}-improver additives is not reported. In any case, fine tuning of the nature and concentration of additives conducted via the chemometric approach allowed us to achieve higher V_{oc} values than those measured for the commercial product.

3.1.6. *Effect of GuSCN additive (x_6)*

Guanidinium thiocyanate (GuSCN) is the most questioned additive in the literature. In particular, several research groups have emphasized its positive effect on photovoltaic performance, while others have stopped using it because it was considered irrelevant or, even, disadvantageous.

GuSCN was initially used not as a liquid electrolyte additive, but in the dye solution: it has been demonstrated that guanidinium cations were adsorbed along with the N3 dye anions on the TiO_2 electrode surface, screening the lateral coulombic repulsion of the sensitizer and facilitating the self-assembly of a compact dye monolayer, thus reducing the dark current and producing a significant improvement in the V_{oc} [52,60]. Zhang et al. discovered a significant enhancement of J_{sc} when guanidinium cations were added into the liquid electrolyte [61]. In particular, a positive shift in the flatband potential of the TiO_2 electrode increased the electron injection yield. Furthermore, guanidinium cations chemisorbed on the TiO_2 surface passivated the surface recombination sites, thus enhancing the electron lifetime in the semiconductor film and improving the V_{oc}.

By means of the FFD-GL DoE, we have investigated the effect of GuSCN (at concentrations between 0 and 0.4 M) on the photovoltaic performance, to assure if it is truly useful introducing this additive in the liquid electrolyte. However, as can be seen in Fig. 2A,

the addition of GuSCN resulted in a large decrease in DSSC efficiency. This effect was due to the decrease of J_{sc} and *FF*, while the V_{oc} was not so much affected. As an example, cells N11 ($x_6 = 0.4$ M) and N12 ($x_6 = 0$ M) can be considered: in the presence of GuSCN, the J_{sc} dropped from 14.5 mA cm^{-2} to 11.9 mA cm^{-2}, while the *FF* was reduced from 0.61 to 0.54.

From these results, it is clear that our chemometric approach highlights the fact that adding GuSCN to the liquid electrolyte is counterproductive to photovoltaic performance. This is consistent with the gradual abandonment of this additive. Furthermore, it has recently been demonstrated that GuSCN-based electrolytes show degradation of photocurrent with time, due to needle-shaped crystals which GuSCN forms on the dye-adsorbed TiO_2 film; in addition, GuSCN has been classified as a potential carcinogenic substance [62].

3.1.7. FFD-GL DoE: final discussion

Through the chemometric approach adopted in this work, it has been possible to evaluate the effect of six important variables related to the composition of liquid electrolytes on the photovoltaic performance of the resulting DSSCs. In summary, we can recapitulate the results as follows:

- Iodide concentration (x_1): it is necessary to adopt a compromise in order to get the highest possible J_{sc} without lowering the V_{oc}. The chemometric model suggests that an optimal concentration of iodide is 0.45 M.
- Iodide counterion (x_2): it has been verified that small cations (Na^+) involve higher J_{sc} but lower V_{oc}, and *vice versa* for counterions with large radius (TBA^+). From a quantitative point of view, the model allowed us to demonstrate that the effect of the increase of J_{sc} is prevalent, thus it is better to use NaI as a source of iodide ions.
- Iodide/iodine molar ratio (x_3): high I^-/I_2 molar ratios decreased *FF* values, while J_{sc} and V_{oc} slightly increased. Quantitatively, the effect on *FF* was predominant, thus a I^-/I_2 molar ratio equal to 8 has been identified as the best choice.
- V_{oc}-improver additives concentration (x_4): it has been shown that it is difficult to significantly increase the photovoltage of DSSCs without sacrificing the photocurrent, thus we can say that a concentration of V_{oc}-improver additives equal to 0.55 M is the best compromise.
- V_{oc}-improver additive type (x_5): from a quantitative point of view, the multivariate investigation of the experimental domain highlighted that the best option is to use TBP rather than NMBI or TBP-NMBI mixtures as V_{oc}-improver additive, due to the fact that − if compared to NMBI − it led to a minor decrease in photocurrent.
- GuSCN additive (x_6): the chemometric model shows that it is counterproductive for DSSC photovoltaic performance.

It can be concluded that the best formulation for a liquid electrolyte for DSSCs is that of cell N18: 0.45 M NaI, 0.056 M I_2 ($I^-/I_2 = 8$) and 0.55 M TBP. We want to emphasize the fact that this formulation is much simpler, more economical and less toxic than those often adopted in the literature, that contain particular kinds of iodine salts, high concentrations of V_{oc}-improver additives and GuSCN. It has been possible to achieve this kind of result only by the above validated and robust multivariate approach, which has been proven to be superposable on the previously published monovariate investigations focused on the single choice of additives and salts for liquid electrolytes.

By studying the behavior of cell N18 under illumination at different light intensities, we observed that the J_{sc} linearly increased from 3.6 mA cm^{-2} (at 0.2 sun) to 16.6 mA cm^{-2} (at 1.0 sun), while the V_{oc} was only slightly improved, as shown in Fig. 4. This linearity assured that neither the I^-/I_3^- transport in the liquid electrolyte nor electron transfer at the Pt/electrolyte interface are rate-determining steps [63]. Moreover, under very low light intensity (0.2 sun), the cell showed an efficiency equal to 7.51%, indicating that the chemometric-tuned electrolyte can ensure an excellent device performance even under not optimal lighting conditions, as well as in indoor environments.

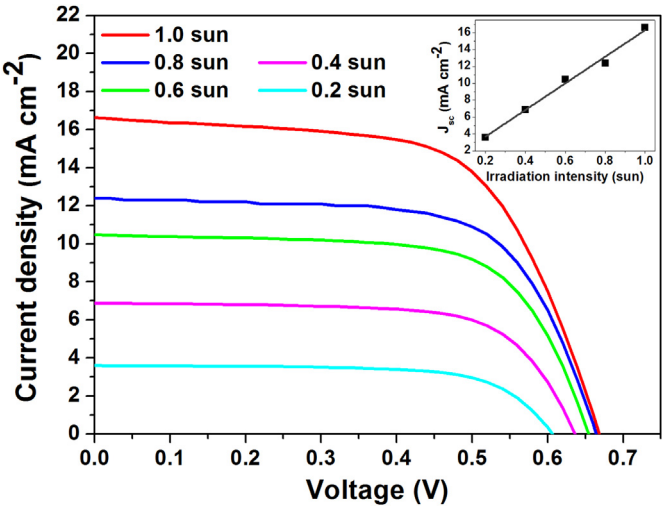

Fig. 4. Photocurrent–photovoltage curves for a DSSC fabricated with the liquid electrolyte N18 (see Table 2) under different light intensities. *Inset*: J_{sc} values plotted as a function of the different light intensities.

3.2. Optimized electrolyte with blocking layer-equipped cell

One of the main disadvantages of the heterogeneous molecular architecture of DSSCs concerns the charge recombination processes which interfere with the unidirectional electron transport. This competitive event extensively occurs at the interface between FTO and the liquid electrolyte which impregnates the mesoporous TiO_2. To overcome this, the scientific community introduced the use of a compact metal oxide blocking layer (BL) between the two above components [64]. Several insulating layers such as TiO_2, Nb_2O_5, ZnO, ZrO_2, SiO_2, Al_2O_3, In_2O_3, MgO have been investigated as BLs. Among these, TiO_2 is the most effective blocker, and has been extensively investigated and deposited using several techniques, such as thermal annealing, pressing, dip coating, hydrolysis of $TiCl_4$ aqueous solution, atomic layer deposition, RF sputtering, and reactive ICP-assisted DC magnetron sputtering [65].

Since the DoE led to the optimization of the electrolyte and of the cathode/electrolyte and TiO_2/dye/electrolyte interfaces, with the aim of improving also the FTO/electrolyte interface we introduced a novel TiO_2 BL. It has been combined with the N18 liquid electrolyte optimized by the multivariate chemometric approach, to see how the photovoltaic performance can be further increased. BL was deposited onto Si substrates and FTO-covered glasses, through the reactive sputtering technique. The morphology and average thickness of TiO_2 film deposited on Si substrate were analyzed by means of FESEM measurements. A fine-grained columnar structure was observed, as shown in Fig. 5. Different regions of the surface were analyzed, showing the presence of a uniform and homogeneous layer. The average thickness was estimated to be around 30 nm.

The crystal structure and orientation of the BL deposited on Si substrate were analyzed by XRD measurements. The appearance of the typical diffraction peak of (110) crystallographic planes,

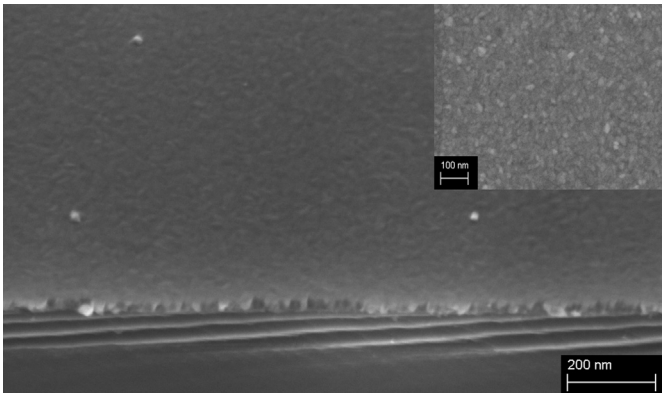

Fig. 5. Cross-sectional FESEM image of TiO_2 BL deposited on silicon substrate. *Inset*: the morphology of the resulting film.

associated to the TiO_2 rutile phase, confirmed the presence of a TiO_2 layer, as shown in Fig. 6 [66]. The broadened shape of the peak can be associated to the presence of mechanical stresses between the BL and the substrate, mainly due to the thinness of the BL and to the lattice mismatch with respect to the Si substrate.

In accordance to the results already reported in the literature [67], our experiments showed that the deposition of the BL onto FTO prior to that of the nanoparticulated TiO_2 was effective in enhancing photovoltaic performances of the DSSC. In Table 4 the photovoltaic parameters of the device fabricated with the BL are compared to the cell with the bare FTO substrate (cell N18 of Table 2); the relative *J–V* curves are reported in Fig. S2. By looking at the results, the enhancement of cell efficiency is mainly to be ascribed to larger photovoltage and *FF* values. This improvement has been attributed to the suppression of the back electron recombination occurring at the substrate surface, thanks to the presence of the compact TiO_2 layer [68]. In our case, in fact, the presence of the BL guaranteed a longer lifetime compared to that of the cell fabricated with the bare FTO: efficiency increased from 6.90% to 8.07%.

For particular purposes, such as flexible cells [69], aerospace applications [70] and power stations [71], cell transparency is not required; therefore, it can be useful to place the cells on reflective surfaces to increase the photon flux incident on the devices. Obviously, this improvement can be obtained only if the electrolyte is able both to effectively regenerate the sensitizer under these particular conditions, and it is not too colored to absorb the light

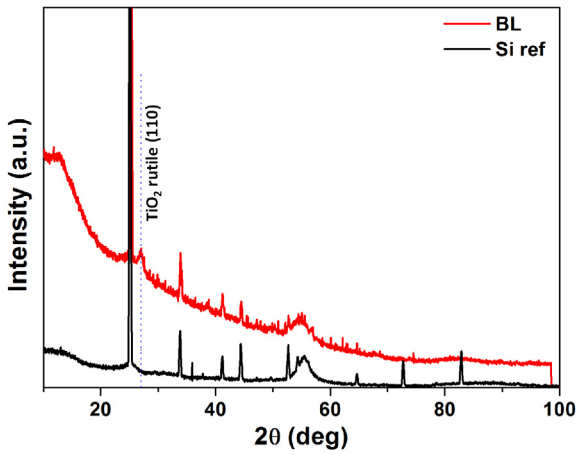

Fig. 6. XRD spectrum of TiO_2 blocking layer deposited on Si.

Table 4
Photovoltaic parameters of DSSCs assembled with the N18 liquid electrolyte (see Table 2), in the presence or in the absence of a TiO_2-based blocking layer (BL). Efficiency values in the presence of the back-reflector (BR) set-up are also reported.

Cell	J_{sc} (mA cm^{-2})	V_{oc} (mV)	*FF*	η (%)	τ_n (ms)	η_{BR} (%)
N18	16.6	668	0.62	6.90	89	8.62
N18 + BL	16.6	706	0.69	8.07	134	10.79

reflected from the reflective surface. To this purpose, in the last column of Table 4 we also report the efficiency of the BL-equipped cell measured with a back-reflector (BR) set-up: in this case the impressive value of 10.79% was obtained, thereby further confirming the high performance of the liquid electrolyte prepared and optimized accordingly to the chemometric method.

4. Conclusions

In this paper, a multivariate chemometric approach has been planned and carried out with the aim of simultaneously studying six fundamental variables to obtain high performance liquid electrolytes for DSSCs. The analysis of the results derived from the fit of the chemometric model allowed us to identify the optimal concentrations of each species present in the formulation, and the results obtained from the *I–V* and EIS characterizations have been interpreted and contextualized to the state of the art.

In previous works, only one component at a time was studied. For the first time, this paper quantifies how effective or not each additive or salt introduced in the electrolyte solution is with respect to the rest of the components. Multivariate analysis allowed us to prepare a final optimal formulation, able to provide an efficiency equal to 6.90% when introduced in a commercial components-based DSSC. This value was improved up to 8.07% when a sputtering-prepared blocking layer was introduced, and further increased up to 10.79% when a light back-reflective surface was used.

The present findings show the importance of multivariate studies in scientific fields where several parameters are relevant. In addition, it has been shown that some commonly used additives or salts are ineffective (or even counterproductive), and their elimination from the liquid electrolyte would help to decrease the cost of the final device.

Acknowledgments

Authors are grateful to Dr. Angelica Chiodoni for her kind assistance in the morphological properties evaluation. Dr. Claudia Barolo is kindly acknowledged for the fruitful discussions.

Appendix A. Supplementary data

Supplementary data related to this article can be found at http://dx.doi.org/10.1016/j.jpowsour.2014.04.088.

References

[1] A.N. Menegaki, Renew. Sustain. Energy Rev. 29 (2014) 31–36.
[2] J. Cochran, T. Mai, M. Bazilian, Renew. Sustain. Energy Rev. 29 (2014) 246–253.
[3] P.C.K. Vesborg, T.F. Jaramillo, RSC Adv. 2 (2012) 7933–7947.
[4] V. Mlinar, Nanotechnology 24 (2013) art. no. 042001.
[5] B. O'Regan, M. Grätzel, Nature 353 (1991) 737–740.
[6] M. Grätzel, J. Photochem. Photobiol. C 4 (2003) 145–153.
[7] M. Wu, X. Lin, T. Wang, J. Qiu, T. Ma, Energy Environ. Sci. 4 (2011) 2308–2315.
[8] J.L. Lan, T.C. Wei, S.P. Feng, C.C. Wan, G. Cao, J. Phys. Chem. C 116 (2012) 25727–25733.

[9] J.F. Yin, M. Velayudham, D. Bhattacharya, H.C. Lin, K.L. Lu, Coord. Chem. Rev. 256 (2012) 3008–3035.
[10] D. Pugliese, F. Bella, V. Cauda, A. Lamberti, A. Sacco, E. Tresso, S. Bianco, ACS Appl. Mater. Interfaces 5 (2013) 11288–11295.
[11] F. Hao, P. Dong, Q. Luo, J. Li, J. Lou, H. Lin, Energy Environ. Sci. 6 (2013) 2003–2019.
[12] F. Bella, A. Sacco, G.P. Salvador, S. Bianco, E. Tresso, C.F. Pirri, R. Bongiovanni, J. Phys. Chem. C 117 (2013) 20421–20430.
[13] H.C. Weerasinghe, F. Huang, Y.B. Cheng, Nano Energy 2 (2013) 174–189.
[14] F. Bella, R. Bongiovanni, J. Photochem. Photobiol. C 16 (2013) 1–21.
[15] C.Y. Hsu, Y.C. Chen, R.Y.Y. Lin, K.C. Ho, J.T. Lin, Phys. Chem. Chem. Phys. 14 (2012) 14099–14109.
[16] M. Wang, C. Grätzel, S.M. Zakeeruddin, M. Grätzel, Energy Environ. Sci. 5 (2012) 9394–9405.
[17] J. Cong, X. Yang, L. Kloo, L. Sun, Energy Environ. Sci. 5 (2012) 9180–9194.
[18] G. Boschloo, A. Hagfeldt, Acc. Chem. Res. 42 (2009) 1819–1826.
[19] S. Yanagida, Y. Yu, K. Manseki, Acc. Chem. Res. 42 (2009) 1827–1838.
[20] Z. Yu, N. Vlachopoulos, M. Gorlov, L. Kloo, Dalt. Trans. 40 (2011) 10289–10303.
[21] A. Lamberti, A. Sacco, S. Bianco, E. Giuri, M. Quaglio, A. Chiodoni, E. Tresso, Microelectron. Eng. 88 (2011) 2308–2310.
[22] A. Sacco, A. Lamberti, D. Pugliese, A. Chiodoni, N. Shahzad, S. Bianco, M. Quaglio, R. Gazia, E. Tresso, C.F. Pirri, Appl. Phys. A 109 (2012) 377–383.
[23] W. Promnopas, T. Thongtem, S. Thongtem, J. Nanomater (2014). Art. ID 529629.
[24] S.W. Gao, Z. Lan, W.X. Wu, L.F. Que, J.H. Wu, J.M. Lin, M.L. Huang, Acta Phys. Chim. Sin. 30 (2014) 446–452.
[25] A. Sacco, A. Lamberti, M. Quaglio, S. Bianco, E. Tresso, A.L. Alexe-Ionescu, C.F. Pirri, Int. J. Photoenergy (2012). Art. ID 216780.
[26] R. Harikisun, H. Desilvestro, Sol. Energy 85 (2011) 1179–1188.
[27] B.K. Lavine, J. Workman Jr., Anal. Chem. 85 (2013) 705–714.
[28] C.F. Mandenius, A. Brundin, Biotechnol. Prog. 24 (2008) 1191–1203.
[29] F.T. Hong, Prog. Biophys. Mol. Biol. 113 (2013) 181–215.
[30] M.C. Yeber, J.A. Cid, Desalin. Water Treat. 51 (2013) 2102–2108.
[31] O. Popescu, R.M. Diaconescu, A. Grigoriu, E. Vasluianu, Ind. Textila 63 (2012) 68–74.
[32] M.M. Carvalho, L.A.M. Ruotolo, R. Fernandez-Felisbino, Microporous Mesoporous Mater. 165 (2013) 163–167.
[33] G.P.H. Styan, C. Boyer, K.L. Chu, Stat. Pap. 50 (2009) 917–941.
[34] Z.R. Lazić, Design of Experiments in Chemical Engineering: a Practical Guide, Wiley-VCH, Weinheim, 2004.
[35] P. Geladi, B.R. Kowalski, Anal. Chim. Acta 185 (1986) 1–17.
[36] L. Vesce, R. Riccitelli, Prog. Photovoltaics Res. Appl. 20 (2012) 960–966.
[37] Z. Lan, J. Wu, D. Wang, S. Hao, J. Lin, Y. Huang, Sol. Energy 80 (2006) 1483–1488.
[38] Y. Rong, X. Li, G. Liu, H. Wang, Z. Ku, M. Xu, L. Liu, M. Hu, Y. Yang, M. Zhang, T. Liu, H. Han, J. Power Sources 235 (2013) 243–250.
[39] Y. Liu, A. Hagfeldt, X.R. Xiao, S.E. Lindquist, Sol. Energy Mater. Sol. Cells 55 (1998) 267–281.
[40] S. Pelet, J.E. Moser, M. Gratzel, J. Phys. Chem. B 104 (2000) 1791–1795.
[41] C.L. Olson, J. Phys. Chem. B 110 (2006) 9619–9626.
[42] H. Wang, L.M. Peter, J. Phys. Chem. C 116 (2012) 10468–10475.
[43] A. Subramanian, J.S. Bow, H.W. Wang, Thin Solid Films 520 (2012) 7011–7017.
[44] S. Sodergren, H. Siegbahn, H. Rensmo, H. Lindstrom, A. Hagfeldt, S.E. Lindquist, J. Phys. Chem. B 101 (1997) 3087–3090.
[45] M.C. Justice, J.C. Justice, J. Solut. Chem. 5 (1976) 543–561.
[46] N. Papageorgiou, M. Grätzel, P.P. Infelta, Sol. Energy Mater. Sol. Cells 44 (1996) 405–438.
[47] T.M.W.J. Bandara, W.J.M.J.S.R. Jayasundara, M.A.K.L. Dissanayake, H.D.N.S. Fernando, M. Furlani, I. Albinsson, B.E. Mellander, Int. J. Hydrogen Energy 39 (2014) 2997–3004.
[48] W. Kubo, S. Kambe, S. Nakade, T. Kitamura, K. Hanabusa, Y. Wada, S. Yanagida, J. Phys. Chem. B 107 (2003) 4374–4381.
[49] J.C. Roy, W.H. Hamill, R.R. Williams, J. Am. Chem. Soc. 77 (1955) 2953–2957.
[50] F. Hao, H. Lin, J. Zhang, D. Zhuang, Y. Liu, J. Li, Electrochim. Acta 55 (2010) 7225–7229.
[51] Z. Yu, M. Gorlov, J. Nissfolk, G. Boschloo, L. Kloo, J. Phys. Chem. C 114 (2010) 10612–10620.
[52] M.K. Nazeeruddin, A. Kay, I. Rodicio, R. Humphry-Baker, E. Mueller, P. Liska, N. Vlachopoulos, M. Grätzel, J. Am. Chem. Soc. 115 (1993) 6382–6390.
[53] X. Xu, E.M. Barea, F. Fabregat-Santiago, J. Bisquert, G. Xu, Proc. SPIE Int. Soc. Opt. Eng. 7518 (2009) art. no. 75180J.
[54] M.K. Nazeeruddin, S.M. Zakeeruddin, R. Humphry-Baker, M. Jirousek, P. Liska, N. Vlachopoulos, V. Shklover, C.H. Fischer, M. Grätzel, Inorg. Chem. 38 (1999) 6298–6305.
[55] G. Boschloo, H. Lindström, E. Magnusson, A. Holmberg, A. Hagfeldt, J. Photochem. Photobiol. A 148 (2002) 11–15.
[56] H. Yang, J. Liu, Y. Lin, J. Zhang, X. Zhou, Electrochim. Acta 56 (2011) 6271–6276.
[57] G. Boschloo, L. Häggman, A. Hagfeldt, J. Phys. Chem. B 110 (2006) 13144–13150.
[58] P.T. Nguyen, P.E. Hansen, T. Lund, Sol. Energy 88 (2013) 23–30.
[59] X.L. Wang, M. Wu, J. Ding, Z.S. Li, K.N. Sun, J. Power Sources 246 (2014) 10–18.
[60] M. Grätzel, J. Photochem. Photobiol. A 164 (2004) 3–14.
[61] C.N. Zhang, Y. Huang, Z.P. Huo, S.H. Chen, S.Y. Dai, J. Phys. Chem. C 113 (2009) 21779–21783.
[62] M.J. Kim, N.G. Park, Appl. Surf. Sci. 258 (2012) 8915–8918.
[63] D. Qin, Y. Zhang, S. Huang, Y. Luo, D. Li, Q. Meng, Electrochim. Acta 56 (2011) 8680–8687.
[64] A.K. Chandiran, M.K. Nazeeruddin, M. Grätzel, Adv. Funct. Mater. 24 (2014) 1615–1623.
[65] S. Vijayalakshmy, B. Subramanian, Electrochim. Acta 116 (2014) 334–342.
[66] A. Vale, N. Chaure, M. Simonds, A.K. Ray, N. Bricklebank, J. Mater. Sci. Mater. Electron. 17 (2006) 851–855.
[67] H. Yu, S. Zhang, H. Zhao, G. Will, P. Liu, Electrochim. Acta 54 (2009) 1319–1324.
[68] J. Xia, N. Masaki, K. Jiang, S. Yanagida, J. Phys. Chem. C 111 (2007) 8092–8097.
[69] V. Zardetto, F. Di Giacomo, D. Garcia-Alonso, W. Keuning, M. Creatore, C. Mazzuca, A. Reale, A. Di Carlo, T.M. Brown, Adv. Energy Mater. 3 (2013) 1292–1298.
[70] J.D. Harris, E.J. Anglin, A.F. Hepp, S.G. Bailey, D.A. Scheiman, S.L. Castro, ESA SP 502 (2002) 629–632.
[71] S. Dai, J. Weng, Y. Sui, S. Chen, S. Xiao, Y. Huang, F. Kong, X. Pan, L. Hu, C. Zhang, K. Wang, Inorg. Chim. Acta 361 (2008) 786–791.